RENAL FAILURE
2026, VOL. 48, NO. 1, 2650263
https://doi.org/10.1080/0886022X.2026.2650263

Taylor & Francis
Taylor & Francis Group

LABORATORY STUDY

OPEN ACCESS Check for updates

Complement activation and fibrinolysis dysregulation drive contrast-induced acute kidney injury: a 4D proteomics rat study

Qiang Yang[a,b,c,d,e#], Liming Sun[f#], Zhijian Zhang[g#], Zhixin Yan[a,b,c,d,e], Jian Zhang[a,b,c,d,e], Jiachang Hu[a,b,c,d,e] and Xiaoqiang Ding[a,b,c,d,e]

[a]Department of Nephrology, Zhongshan Hospital, Fudan University, Shanghai, China; [b]Shanghai Medical Center of Kidney, Shanghai, China; [c]Shanghai Institute of Kidney and Dialysis, Shanghai, China; [d]Shanghai Key Laboratory of Kidney and Blood Purification, Shanghai, China; [e]Hemodialysis Quality Control Center of Shanghai, Shanghai, China; [f]Shanghai Clinical Research and Trial Center, ShanghaiTech University, Shanghai, China; [g]Department of Nephrology, The Affiliated Wuxi People's Hospital of Nanjing Medical University, Wuxi People's Hospital, Wuxi Medical Center, Nanjing Medical University, Wuxi, Jiangsu, China

ABSTRACT

Contrast-induced acute kidney injury (CI-AKI) is a major cause of hospital-acquired AKI, but its molecular pathogenesis remains incompletely understood. In this study, we used quantitative 4D proteomics, integrating ion mass-to-charge ratio (m/z), retention time, ion intensity, and ion mobility, to profile renal tissues from a novel rat CI-AKI model based on renal venous congestion and contrast exposure, with sham-operated rats as controls. Differentially expressed proteins were identified and analyzed using pathway enrichment and protein–protein interaction (PPI) network approaches, followed by experimental validation. Using nominal screening criteria ($|\log2FC| \geq 1.5$ and $p < 0.05$), we identified 180 candidate differentially expressed proteins, including 92 upregulated and 88 downregulated proteins. Pathway-level analyses showed coordinated upregulation of complement-related proteins, including C3/C5 convertase-related components and terminal pathway proteins, such as C9, together with a C4 isoform annotated as C4a in the reference database. Coagulation and fibrinolysis pathways were also markedly altered, including fibrinogen chains (FGA, FGB, FGG), PLAU, SERPINA1, and SERPINF2. In contrast, proteins associated with AMPK and MAPK signaling (including HNF4α, PRKAA2, PRKAB1, and MAP2K3) were reduced. These pathway-level changes were supported by RT-qPCR and immunohistochemical analyses. Collectively, our findings support a multidimensional injury network in rat CI-AKI involving complement activation, coagulation–fibrinolysis dysregulation, and impaired metabolic/stress-response signaling, and provide a proteomic resource for future mechanistic and translational studies.

GRAPHICAL ABSTRACT

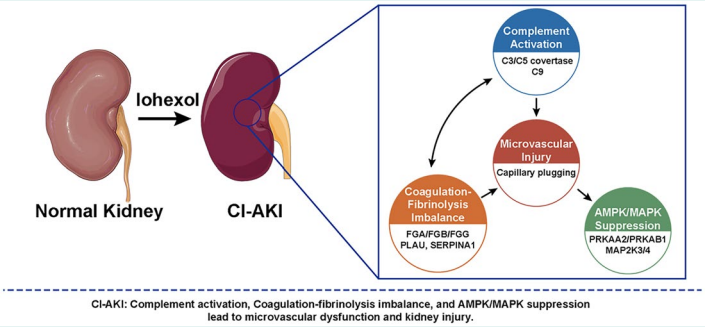

ARTICLE HISTORY

Received 26 November 2025
Revised 25 February 2026
Accepted 20 March 2026

KEYWORDS

Contrast-induced acute kidney injury; complement activation; coagulation and fibrinolysis; proteomics; acute kidney injury biomarkers; mitochondrial dysfunction

CONTACT Xiaoqiang Ding ding.xiaoqiang@zs-hospital.sh.cn; Jiachang Hu hu.jiachang@zs-hospital.sh.cn Department of Nephrology, Zhongshan Hospital, Fudan University,180, Fenglin Road, Xuhui District, Shanghai 200032, China
[#]These authors contributed equally to this work.

Supplemental data for this article can be accessed online at https://doi.org/10.1080/0886022X.2026.2650263.

1. Introduction

The increased use of contrast media in medical imaging [1], especially for coronary intervention and other contrast-intensive procedures, has led to a growing number of patients who develop contrast-induced acute kidney injury (CI-AKI) [2], and a substantial proportion of these patients subsequently develop chronic kidney disease (CKD) or experience persistent renal dysfunction [3]. CI-AKI is typically defined as an increase in the serum creatinine (SCr) level of more than 1.5-fold above baseline or as an absolute increase of more than 26.5 µmol/L (0.3 mg/dL) within 2 d after contrast injection [4]. Although the precise pathophysiology of CI-AKI remains incompletely understood, current evidence implicates direct tubular cytotoxicity, hemodynamic disturbances, and oxidative stress as key contributors [5–8].

Existing studies have primarily focused on interrelated mechanisms such as hemodynamic disturbances and tubular injury [2,6, 9–12]. However, these single-pathway models have significant limitations. They fail to adequately explain the heterogeneous clinical manifestations observed across different patient populations [13], and the crosstalk between hemodynamic perturbations and the hierarchical signaling networks governing cellular injury remains poorly characterized [14,15]. These knowledge gaps likely hinder the identification of effective therapeutic targets [16]. To address this complexity and capture the multifaceted nature of CI-AKI pathophysiology, a systems-level approach is critically needed. Proteomics enables the systematic characterization of global protein expression profiles, protein–protein interaction (PPI) networks, and pathway dynamics through high-throughput analysis. This approach offers a powerful framework for capturing pathway crosstalk and identifying hub regulators in complex diseases, and has proven valuable for elucidating pathophysiological processes in kidney disorders [17–19].

In this study, we employed 4D proteomics – including measurements of ion mass-to-charge ratio (m/z), retention time, ion intensity, and ion mobility – to compare renal tissues from rats with CI-AKI and control, with the aim of identifying differentially expressed proteins and dysregulated pathways associated with CI-AKI pathophysiology. By generating a systems-level map of injury-associated molecular programs, this study seeks to advance mechanistic understanding of CI-AKI and provide a foundation for subsequent translational investigations.

2. Materials and methods

2.1. Chemicals and antibodies

Renal injury was induced by the administration of iohexol (350 mgI/mL; GE Healthcare, Shanghai, China; catalog no. HJ20160023), a nonionic low-osmolar contrast agent. Primary antibodies used for immunohistochemistry (IHC) included anti-NOX4, anti-TNF-α, anti-CD68, anti-Ly6G, anti-C3, and anti-fibrinogen β chain (FGB) antibodies. The sources, catalog numbers, and working dilutions are listed below: NOX4 (cat. no. GB11347, 1:1000, Servicebio, Wuhan, China); TNF-α (cat. no. GB11188, 1:200, Servicebio, Hubei, China); CD68 (cat. no. GB113109, 1:100, Servicebio); Ly6G (cat. no. 14-5931-82, 1:50, Thermo Fisher Scientific, Waltham, MA); C3 (cat. no. sc-28294, 1:50, Santa Cruz Biotechnology, Dallas, TX); and FGB (cat. no. 16747-1-AP, 1:50, Proteintech, Rosemont, IL). The HRP-conjugated secondary antibody (cat. no. G1213, Servicebio) and the DAB substrate kit (cat. no. G1212, Servicebio) were used for detection.

Commercial assay kits for SCr and blood urea nitrogen (BUN) were purchased from BioAssay Systems, Hayward, CA (cat. no. DICT-500 and DIUR-100). ELISA kits for neutrophil gelatinase-associated lipocalin (NGAL) and kidney injury molecule-1 (KIM-1) were obtained from Abcam, Cambridge, UK (catalog nos. ab119602 and ab119597). CellROX® Red reagent (catalog no. C10422, Thermo Fisher Scientific), DAPI (catalog no. D1306, Thermo Fisher Scientific), TUNEL assay kit (catalog no. A113-02, Vazyme Biotech, Nanjing, China), TRIzol reagent (catalog no. 93289, Sigma-Aldrich), PrimeScript RT reagent kit (catalog no. RR037A, TaKaRa, Japan), and qPCR master mix (catalog no. RR420A, TaKaRa, Japan) were used in this study. Masson's Trichrome staining kit (Sigma-Aldrich, St. Louis, MO, HT15) and Martius Scarlet Blue (MSB) staining kit (Solarbio, Cat. No. G2040) were used for histological analyses.

2.2. Establishment and validation of a novel CI-AKI rat model

The CI-AKI model was established based on a previously reported protocol that integrates renal venous congestion and contrast exposure [12]. Male Sprague-Dawley rats (180–200 g) were obtained from Shanghai B&K Experimental Animal Center. All procedures were approved by the Institutional Animal Care and Use Committee of Fudan University (ethical approval number:2019-210) and complied with the NIH Guide for the Care and Use of Laboratory Animals. Rats were randomly allocated into CI-AKI and sham groups. A total of eight male Sprague-Dawley rats (180–200 g) were randomly assigned to two groups: the CI-AKI group ($n=4$) and the Sham group ($n=4$) using a lottery drawing method. The sample size was determined based on previous experience with similar models and pilot studies. The CI-AKI group underwent 15-min occlusion of the left renal vein, contralateral nephrectomy, and tail vein injection of 15 mL/kg iohexol. Sham-operated rats received normal saline instead of contrast. Blood was collected at baseline and 24 h post-procedure. SCr and BUN were measured using commercial kits (BioAssay Systems). Kidney injury was further assessed *via* serum NGAL and KIM-1 levels using ELISA kits (Abcam). Rats were euthanized with sodium pentobarbital (150 mg/kg, i.p.), and renal tissues were harvested for subsequent analysis.

2.3. Sample preparation for LC–MS/MS

For the comprehensive 4D LC–MS/MS proteomic analysis, renal cortical tissues from three randomly selected rats in each group were used. All eight animals were utilized for the assessment of renal function (SCr, BUN), tubular injury markers (NGAL, KIM-1), and histopathological evaluation (H&E, IHC, etc.). The exact sample size (n) for each specific statistical analysis is detailed in the corresponding figure legends. For proteomics analysis, the renal tissues of the other three rats in each group were stored at −80 °C.

2.3.1. Sample preparation for mass spectrometry-based proteomics

Protein digestion was conducted following the filter-aided sample preparation (FASP) method using 10 kDa molecular weight cutoff centrifugal filters (Pall Corporation), as previously described [20]. Briefly, the renal tissues from rat were homogenized in SDT lysis buffer containing 4% (w/v) SDS, 100 mM Tris, and 100 mM DTT (pH 7.6), followed by sonication and centrifugation at 16,000 × g for 10 min. Aliquots of 25 µg protein were diluted with 8 M urea in Tris–HCl (UA buffer) and centrifuged at 12,000 × g for 15 min. Alkylation was performed using 14 mM iodoacetamide in the dark for 20 min. Subsequent steps included washing with UA buffer and buffer exchange into 50 mM ammonium bicarbonate. Trypsin digestion was carried out at a 1:50 (protein:trypsin) ratio, with incubation at 37 °C under gentle agitation for 16 h. The resulting peptides were collected *via* centrifugation, desalted using C18 StageTips (3 M), and dried in a vacuum concentrator.

2.3.2. Liquid chromatography and tandem mass spectrometry (LC–MS/MS)

LC-MS/MS analyses were performed on a timsTOF Pro mass spectrometer (Bruker Daltonics) coupled to an UltiMate 3000 RSLCnano system (Thermo Scientific). Peptides were injected and separated on a reversed-phase capillary column (C18, 1.9 µm, 75 µm × 300 mm) maintained at 55 °C. The mobile phases consisted of 0.1% formic acid in water (solvent A) and 0.1% formic acid in acetonitrile (solvent B). Peptides were eluted using a 60-min nonlinear gradient: 4–23% B (0–45 min), 23–32% B (45–52 min), 32–95% B (52–56 min), and 95% B (56–60 min), at a constant flow rate of 400 nL/min.

Data were acquired in data-independent acquisition parallel accumulation–serial fragmentation (diaPASEF) mode. Full-scan MS spectra were collected from 300 to 1700 m/z, with diaPASEF scans covering 400–1000 m/z using 40 m/z isolation windows. Collision energy settings varied linearly with ion mobility values, ranging from 59 eV at 1.6 Vs/cm^2 to 20 eV at 0.6 Vs/cm^2. The ion mobility range was set from 0.59 to 1.6 Vs/cm^2 with a ramp time of 100 ms.

2.3.3. MS data processing and bioinformatics

Raw diaPASEF data were processed using Spectronaut (v15.6.211220.50606; Biognosys) with default settings, searching against the UniProt Rattus norvegicus reference proteome (reviewed database,

8219 entries, 2024 release). The database search was conducted with the following parameters: fixed modification of carbamidomethyl (C); variable modifications of oxidation (M) and N-terminal acetylation; the protease was set to Trypsin/P with a maximum of 2 missed cleavages permitted. For false discovery rate (FDR) control, a threshold of 1% was set for spectra (PSM), peptides, and protein groups.

2.4. Bioinformatics

For data preprocessing, normalization was performed using the median intensity value within each sample. Differential expression analysis between two groups was carried out using Student's t-test, with significance defined as $p < 0.05$ and a fold change > 1.5. Functional annotation of differentially expressed proteins was performed through Gene Ontology (GO) and KEGG enrichment analysis using the DAVID [21], and p values were adjusted using the FDR approach. All data processing and statistical analyses were conducted in the R environment (version 4.1.2).

PPI networks were analyzed using STRING database version 11.0. A high-confidence interaction was defined as a STRING confidence score > 0.7. Network visualization was generated using the R package networkD3.

2.5. Evaluation of tubular injury by H&E staining

Renal tissues were fixed in 10% neutral-buffered formalin, embedded in paraffin, and sectioned at 3 µm thickness. Hematoxylin and eosin (H&E) staining was performed to evaluate histopathological changes. Sections were examined by two blinded pathologists using a Leica DM 6000 B microscope. Tubular injury – characterized by foamy degeneration, epithelial detachment, and necrosis – was semiquantitatively scored across 10 corticomedullary fields (×200) based on the percentage of affected tubules: 0 (none), 1 (<25%), 2 (25–49%), 3 (50–75%), and 4 (>75%).

2.6. Detection of oxidative stress by CellRox, MDA, SOD, CAT, and GSH-Px

Oxidative stress was evaluated using CellROX® Red Reagent (catalog no. C10422, Thermo Fisher Scientific) on frozen kidney sections. Sections were incubated with 5 µM CellROX® Red reagent at 37 °C for 30 min in the dark, followed by counterstaining with DAPI (1 µg/mL, catalog no. D13022, Thermo Fisher Scientific) for 5 min at room temperature. After washing, images were captured with a Nikon C2 confocal microscope and analyzed with ImageJ. ROS-positive cells were quantified across 10 high-power fields. Lipid peroxidation and antioxidant capacity were further evaluated in renal tissue homogenates by measuring malondialdehyde (MDA), superoxide dismutase (SOD), catalase (CAT), and glutathione peroxidase (GSH-Px) using commercial assay kits (catalog nos. KTB9050-S, KTB1030, KTB1040, and KTB1640, respectively; Abbkine, Wuhan, China) according to the manufacturers' instructions. Results were normalized to total protein concentration, which was determined using a BCA protein assay kit (catalog no. KTD3001, Abbkine).

2.7. Detection of apoptosis by TUNEL assay on confocal laser scanning microscope

Apoptosis was detected using a TUNEL assay kit (Vazyme Biotech). TUNEL-positive and total cells were counted on confocal images (Nikon C2), and the apoptotic index was calculated using ImageJ.

2.8. Immunohistochemical analysis of inflammation, oxidative stress, complement activation, and fibrin deposition

Immunohistochemical (IHC) staining was performed on paraffin-embedded kidney sections using primary antibodies against TNF-α, CD68, Ly6G, NOX4, C3, and fibrinogen β chain (FGB). TNF-α, CD68, and Ly6G were used to assess inflammatory responses and immune cell infiltration, NOX4 was used as a marker of oxidative stress, C3 was used to evaluate complement activation, and FGB immunostaining was

performed to assess fibrinogen deposition and immunothrombotic microvascular involvement. Stained areas were quantified using ImageJ software (National Institutes of Health, Bethesda, MD) and expressed as the percentage of positively stained area per field.

2.9. Detection of mitochondria by transmission electron microscopy

Renal ultrastructure was examined using a Hitachi 7700 transmission electron microscope. For ultrastructural observation, tissue samples underwent fixation in 2.5% glutaraldehyde and staining with uranyl acetate and lead citrate prior to imaging. Mitochondrial morphology was analyzed using ImageJ.

2.10. RNA extraction and quantitative real-time PCR

Total RNA was isolated from renal tissue using TRIzol reagent (Sigma-Aldrich) following standard extraction procedures. The Prime Script RT reagent Kit (TaKaRa, Japan) was used to generate first-strand cDNA. Quantitative real-time PCR was carried out in accordance with the manufacturer's instructions: 40 cycles of denaturation at 95 °C for 5 s and annealing at 60 °C for 34 s. The primer sequences used are listed in the following.

Genes	Forward	Reverse
Gapdh	GGCAAGTTCAACGGCACAGTC	TCGCTCCTGGAAGATGGTGATG
C3	GCTGCCAACCTCATCGCCATC	TGAATCACTGGTCCGTCCTCCTG
C9	AGCAGACGCCCTCCTACCAATAG	TCTCCCAAAGCATCAGCACAGC
Fga	AATGGCAGATGAGGCAGCAAGTG	TGGGCACCTGAAGGATGTGTTTG
Fgb	CAGCCTGACACCTCCAGCAAAC	GCCATCCTGACGGTTCTGTATGAC
Fgg	AATGGCTGGACCGTATTGCA	CAGCCAAAACTCTGTGGTGC
Plau	CATTCGAAGATGCAGCTGCC	CCGGCCTTTGGTGTCAGTAT
Serpina1	CTCATTTCCCGGTTCCTGCT	TGTTGAAGACCCGGGTGATG
Serpinf2	ACTCTGTACCAGCCCTCGAT	GGAACAAGTCCTGTAGGCCC
Prkaa2	ATGATGAGGTGGTGGAGCAGAGG	GGTTCTCGGCTGTGCTGGAATC
Prkab1	CCATCCTCCCGCCTCACCTG	GCACTGAGCACCATCACTCCATC
Hnf4a	GTGCCCTGTGTGCCATCTGTG	TCACGCTCCTCCTGAAGAATCCC
Map2k4	GTGACTTCGGCATCAGTGGACAG	CCCCAAACTCCAGACATCAGAGC

2.11. Masson's Trichrome staining

Serial 4-μm-thick paraffin sections were stained using a Masson's Trichrome kit (Sigma-Aldrich, HT15) according to the manufacturer's instructions. In brief, after deparaffinization and rehydration, the sections were sequentially stained with Weigert's hematoxylin (10 min), Biebrich scarlet-acid fuchsin (10 min), differentiated in phosphomolybdic-phosphotungstic acid, and counterstained with aniline blue (5 min) before dehydration and mounting. The stained sections were then observed under a light microscope (Nikon Eclipse 80i), and at least 10 non-overlapping cortical fields per kidney were captured at 200× magnification. The collagen volume fraction (CVF), defined as the percentage of blue-stained collagen area relative to the total interstitial area (excluding glomeruli and large vessels), was quantified from these images using ImageJ software by an observer blinded to the experimental groups.

2.12. Martius scarlet blue (MSB) staining

MSB staining was performed using a commercial fibrin stain kit (modified MSB method; Solarbio, Cat. No. G2040). Briefly, paraffin-embedded kidney sections were deparaffinized and rehydrated to distilled water, followed by treatment with hypo solution for 3–5 min. Sections were sequentially stained with Celestite Blue solution and Mayer's hematoxylin, differentiated with acidic differentiation solution, and blued under running tap water. Subsequently, sections were stained with Mathew Yellow solution and Acid Red solution, followed by phosphotungstic acid treatment to remove nonspecific collagen staining. Aniline Blue solution was then applied to visualize collagen fibers. After weak acid rinsing, sections were rapidly dehydrated through graded ethanol, cleared in xylene, and mounted with neutral resin. Following MSB staining, fibrin was visualized as red (fresh fibrin may appear yellow, whereas older fibrin may appear blue), nuclei appeared blue-gray, erythrocytes yellow, and collagen fibers blue.

2.13. Statistical analysis

All statistical analyses and graphical representations were conducted using GraphPad Prism version 7.0 (GraphPad Software, San Diego, CA). Continuous variables were expressed as mean ± standard error of the mean (SEM) and compared by a t-test between two groups. Tubular injury scores (ordinal data) were compared using the Mann–Whitney U test. Statistically significant differences were defined as a p value < 0.05.

3. Results

3.1. Establishment of the CI-AKI rat model

After collection of baseline blood samples, we established the CI-AKI rat model by application of unilateral left renal vein clamping (15 min) and contralateral nephrectomy, followed by injection of contrast medium (or NS in the control), and collection of blood and euthanasia after 24 h (endpoint). At the endpoint, the CI-AKI group exhibited a significant impairment in glomerular filtration function, indicated by increased SCr and BUN (Figure 1(A)), alongside a rise in the specific tubular damage markers NGAL and KIM-1 (Figure 1(B)). These biochemical alterations were consistent with the histopathological findings, which revealed tubular epithelial cell swelling and vacuolar degeneration in the CI-AKI group, in contrast to the normal renal architecture seen in the Sham group (Figure 1(C)), collectively confirming successful model establishment.

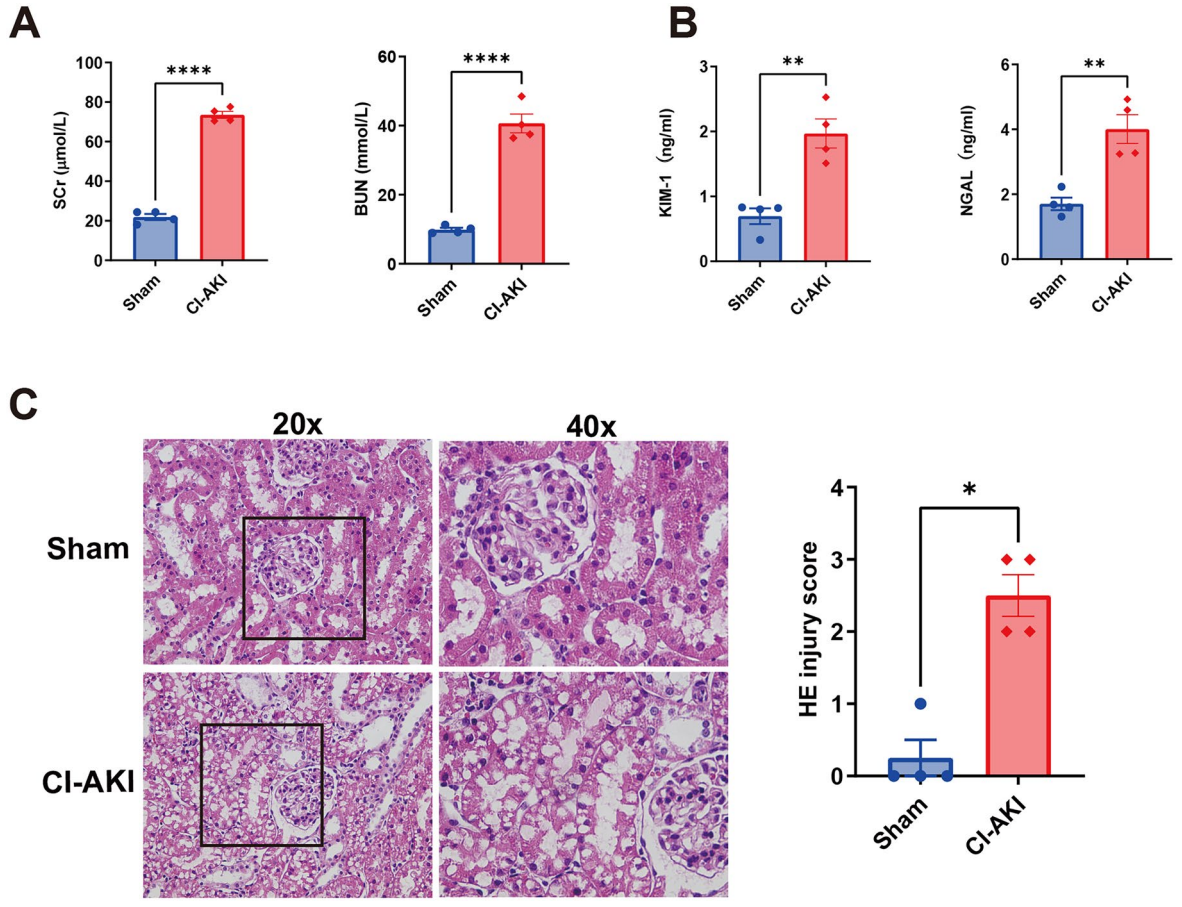

Figure 1. Establishment of the rat model of CI-AKI. AKI blood biomarkers (A, B), H&E staining of renal tissues (C), and H&E renal injury scores in the control group and the CI-AKI group at 24 h after injection of iohexol or NS. Data are expressed as mean ± SEM. Independent-sample t test and Kruskall-Wallis test ($n = 4$ per group *$p < 0.05$, **$p < 0.01$, and ***$p < 0.001$).

3.2. Identification of DEPs

Proteomic analysis by 4D LC–MS/MS identified 46,977 peptides and 5,372 proteins, with PCA showing clear separation between groups and tight clustering of replicates, indicating high reproducibility and distinct proteomic profiles (Figure 2(A)). Heatmap analysis (Figure 2(B)) of the differentially expressed

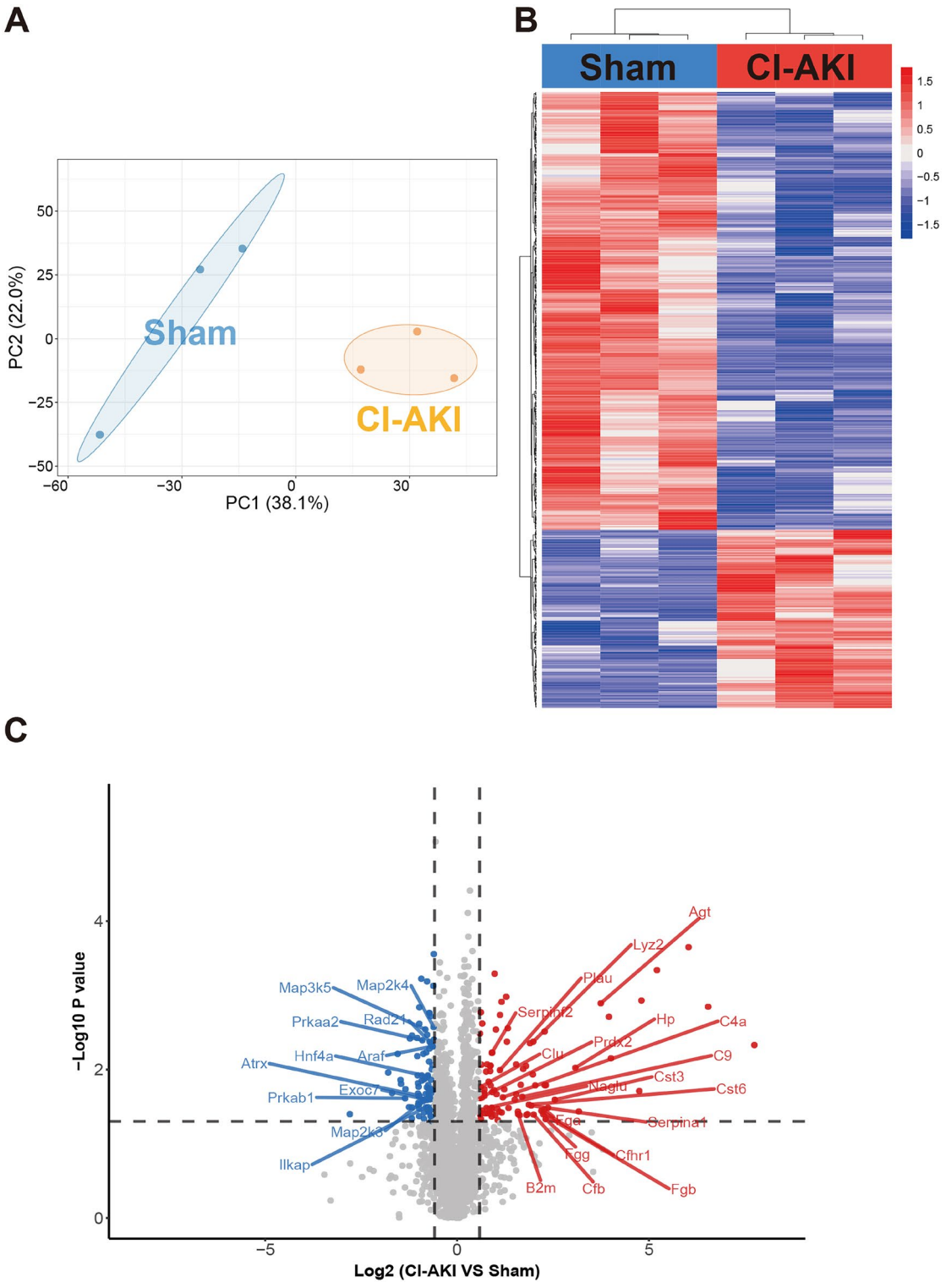

Figure 2. Effect of CI-AKI on the proteome of rat renal tissues. Principal component analysis of the proteomes of the 3 rats in each group (A), protein clustering heatmaps of the two groups (B), and volcano plot of significantly upregulated and downregulated proteins in the CI-AKI group relative to the control group (C).

proteins reinforced the PCA findings. Further quality assessment revealed that 83% of peptides were 7–20 amino acids long, 89% of proteins were supported by ≥2 peptides, 62% had sequence coverage <30%, and protein molecular weights were broadly distributed (Supplementary Figure S2(A–D)), collectively confirming a high-quality and unbiased proteome dataset.

A conventional t-test on log2-transformed protein intensities was used to screen candidate differentially expressed proteins (DEPs) between the CI-AKI and Sham groups, using nominal criteria of |log2FC| >= 1.5 and $p < 0.05$. This screening yielded 180 candidate DEPs (92 upregulated and 88 downregulated; Figure 2(C)).

Tables 1 and 2 show the 20 most significantly up-regulated and downregulated proteins. Notably, the 180 DEPs include 10 traditional and novel biomarkers associated with kidney injury: cystatin-C (CST3) [22], beta-2-microglobulin (β2M) [23], angiotensinogen (AGT) [24], clusterin (CLU) [25], N-acetyl-alpha-glucosaminidase (NAG, NAGLU) [26], alpha-1-antiproteinase (SERPINA1) [27], 1,4-beta-N-acetylmuramidase (NGAL, LYZ2), cystatin E/M (CST6) [28], haptoglobin (HP) [29], and peroxiredoxin-2 (PRDX2) [30].

3.3. Functional enrichment of DEPs

3.3.1. GO and KEGG enrichment analyses

We performed Domain, GO, and KEGG enrichment analyses for further analysis of the significantly upregulated and downregulated proteins in the CI-AKI group. Analysis of the upregulated proteins (Figure 3(A)) demonstrated significant enrichment in biological processes related to complement activation (Figure 3(B)) and the coagulation and fibrinolysis pathways (Figure 3(C)), suggesting upregulation of the complement system and an imbalance of coagulation and fibrinolysis during CI-AKI. Specifically, activation of the alternative complement pathway components (C3/C5 convertase-related proteins and terminal pathway components such as C9) together with the increased abundance of a C4 isoform annoted as C4a is known to increase inflammation [31], oxidative stress [32], and cellular death [33]. Similarly, upregulation of fibrinogen α, β, and γ chains (FGA, FGB, FGG) and the plasminogen activator (PLAU) increases deposition of fibrin, obstructs the peritubular capillaries [34], and aggravates CI ischemia and hypoxia [35]. Upregulation of proteins in the serpin family can inhibit plasmin and further exacerbate microthrombosis [36,37] (Figure 3(D)).

Analysis of the downregulated proteins in CI-AKI demonstrated enrichment in AMPK- and MAPK-associated pathways (Figure 3(E)). In particular, downregulation of HNF4α and AMP (PRKAA2/PRKAB1) can lead to mitochondrial dysfunction [38], decreased production of ATP [39], and increased oxidative stress [40] and lipid peroxidation [41,42] (Figure 3(F)). Suppression of components of the MAPK

Table 1. Twenty proteins with the greatest up-regulation in the renal tissues of CI-AKI rats.

Accession	Protein description	Gene	Average fold change (CI-AKI/Sham)	*p* Value
A0A140UHX6	Spectrin beta chain	Sptb	214.902	0.0047
D4A678	Spectrin	Spta1	93.146	0.0014
B0BNN3	Carbonic anhydrase 1	Ca1	65.372	0.0002
P11517	Hemoglobin subunit beta-2	--	36.967	0.0005
P01946	Hemoglobin subunit alpha-1/2	Hba1	27.925	0.0012
P47967	Galectin-5	Lgals5	26.855	0.0195
Q63910	Alpha globin	Hba-a3	16.096	0.0070
A0A0H2UHI5	Serine protease inhibitor A3N	Serpina3n	15.541	0.0019
P01015	Angiotensinogen	Agt	13.386	0.0013
D3Z9Z0	Ankyrin 1	Ank1	9.012	0.0367
A0A0H2UHM3	Haptoglobin	Hp	8.466	0.0095
P14841	Cystatin-C	Cst3	5.838	0.0256
M0R979	Thrombospondin 1	Thbs1	5.175	0.0326
Q68FY4	Gc-globulin	Gc	4.969	0.0162
P02680	Fibrinogen gamma chain	Fgg	4.942	0.0463
P20059	Hemopexin	Hpx	4.858	0.0162
Q3KR94	Vitronectin	Vtn	4.854	0.0031
Q7TQ70	Fibrinogen alpha chain	Fga	4.852	0.0342
P14480	Fibrinogen beta chain	Fgb	4.749	0.0400
Q5I0M3	Complement component factor h-like 1	Cfhr1	4.582	0.0359

Table 2. Twenty proteins with the greatest downregulation in the renal tissues of CI-AKI rats.

Accession	Protein description	Gene	Average fold change (CI-AKI/Sham)	*p* Value
D4A1J3	Paralemmin 3	Palm3	0.144	0.0398
F1M654	RCG31049	Smim1	0.288	0.0109
P39069	Adenylate kinase isoenzyme 1	Ak1	0.309	0.0207
A0A0H2UHG4	Cyclin-dependent kinase 18	Cdk18	0.342	0.0062
A0A0G2JSQ3	Solute carrier family 22 (Organic anion transporter)	Slc22a8	0.36	0.0138
Q76EQ0	Serine racemase	Srr	0.363	0.0156
P80386	5′-AMP-activated protein kinase subunit beta-1	Prkab1	0.391	0.0244
F1LNL0	APOBEC1 complementation factor	A1cf	0.393	0.0183
G3V7J2	Interferon-inducible double-stranded RNA-dependent protein kinase activator A	Prkra	0.42	0.0320
P45380	Sulfate anion transporter 1	Slc26a1	0.427	0.0038
F7ES73	Negative regulator of ubiquitin-like proteins 1	Nub1	0.442	0.0323
Q6AY94	Complex I assembly factor TIMMDC1 GN = Timmdc1 PE = 2 SV = 1	Timmdc1	0.442	0.0455
Q9JID1	Programmed cell death protein 4	Pdcd4	0.443	0.0035
Q66H66	RAB11 family-interacting protein 3	Rab11fip3	0.486	0.0038
M0RA08	Perilipin	Plin3	0.488	0.0066
F1M8Y4	DEP domain-containing MTOR-interacting protein	Deptor	0.49	0.0120
B1H230	Dual-specificity mitogen-activated protein kinase kinase 3-like	Map2k3	0.494	0.0302
F1M866	Sorbin and SH3 domain-containing protein 1	Sorbs1	0.494	0.0210
B4F7F3	ARVCF	Arvcf	0.495	0.0152
A0A1W2Q6M4	Uncharacterized LOC108348190 (Fragment)	LOC108348190	0.498	0.0279

pathway (MAP2K3, MAP2K4 and MAP3K5) may reflect compromised stress-adaptation and repair signaling [43](Figure 3(G)).

These findings suggest that iohexol treatment induced diverse and multidimensional damage in the renal tubular epithelial cells of rats with CI-AKI, which is associated with complement activation, fibrinolytic imbalance, impaired energy metabolism, and dysregulated stress responses.

3.3.2. Protein–protein interaction network analysis

Protein function is often dependent on the formation of a PPI network. We therefore analyzed DEPs using established criteria and the STRING (version 11.0) database to characterize PPI network in CI-AKI (Figure 4).

The PPI network analysis highlighted coordinated changes in complement-related proteins (including C3/C5 convertase-related components and terminal pathway proteins such as C9, a C4 isoform annotated as C4a) and coagulation-fibrinolysis proteins (FGA, FGB, FGG, PLAU, SERPINA1, SERPINF2), alongside reduced abundance of AMPK- and MAPK-associated signaling nodes (HNF4α, PRKAA2/PRKAB1, MAP2K3/4, A-RAF). Together, these patterns are compatible with a coupled inflammatory-hemostatic response and impaired metabolic/stress adaptation in tubular epithelium, which may contribute to microvascular dysfunction and hypoxic stress during CI-AKI.

3.4. Verification of the LC–MS/MS results

3.4.1. Complement activation

RT-qPCR of renal tissues also indicated there was significant upregulation of the *C3* and *C9* mRNAs in CI-AKI rats (Figure 5(A)), consistent with the LC–MS/MS results. Similarly, IHC demonstrated significant deposition of C3 in the renal tubules of CI-AKI rats, with localization in areas of tubular injury (Figure 5(B)). The CI-AKI kidneys had elevated levels of NOX4 (a ROS-generating enzyme) and cytochrome C (CYT-C, mitochondrial marker of apoptosis) and increased apoptosis, based on the TUNEL assay (Figure 5(C–E)). IHC showed greater infiltration of CD68+ macrophages and LY6G+neutrophils in CI-AKI kidneys and greater expression of TNF-α in the tubular epithelial cells of CI-AKI rats (Figure 5(F–H)).

3.4.2. Fibrinogen expression

RT-qPCR of renal tissues confirmed significant overexpression of Fga, Fgb, Fgg, and Plau in CI-AKI kidneys (Figure 6(A)), consistent with the LC–MS/MS findings. In parallel, FGB IHC showed increased

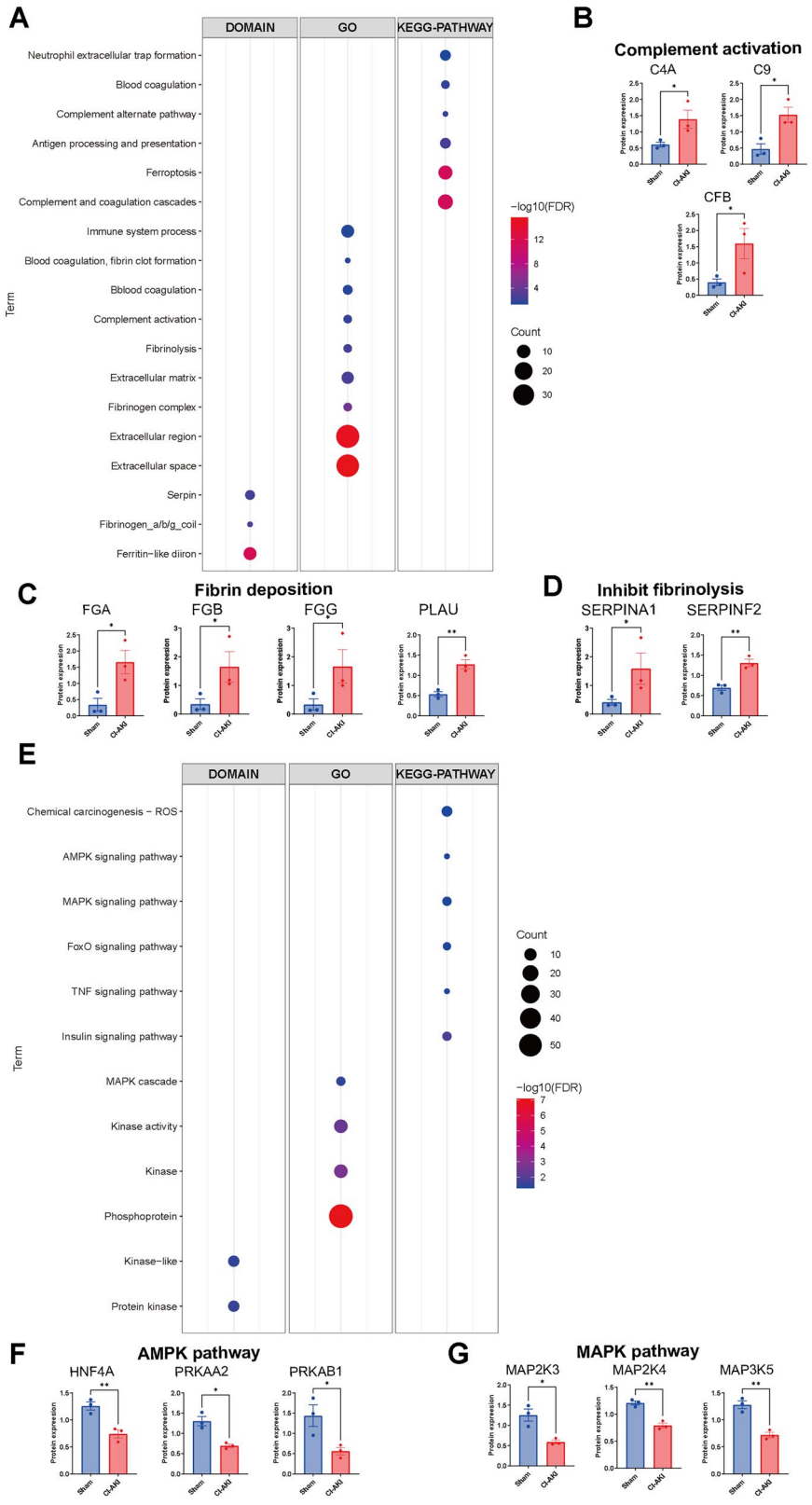

Figure 3. Effect of CI-AKI on enrichment/depletion of proteins in rat renal tissues based on Domain analysis, GO analysis and KEGG analysis. Domains, pathways, processes, and proteins upregulated in CI-AKI rats (A), protein expression of a C4 isoform (annotated as C4a in the database), C9 and CFB (B), protein expression of FGA, FGB, FGG, and PLAU (C), protein expression of SERPINA1 and SERPINF2 (D). Downregulated in CI-AKI rats (E), protein expression of HNF4A, PRKAA2 and PRKAB1 (F) and protein expression of MAP2K3, MAP2K4 and MAP3K5 (G). Data are expressed as mean ± SEM. Independent-sample t test ($n = 3$ per group $^{*}p < 0.05$, $^{**}p < 0.01$, and $^{***}p < 0.001$).

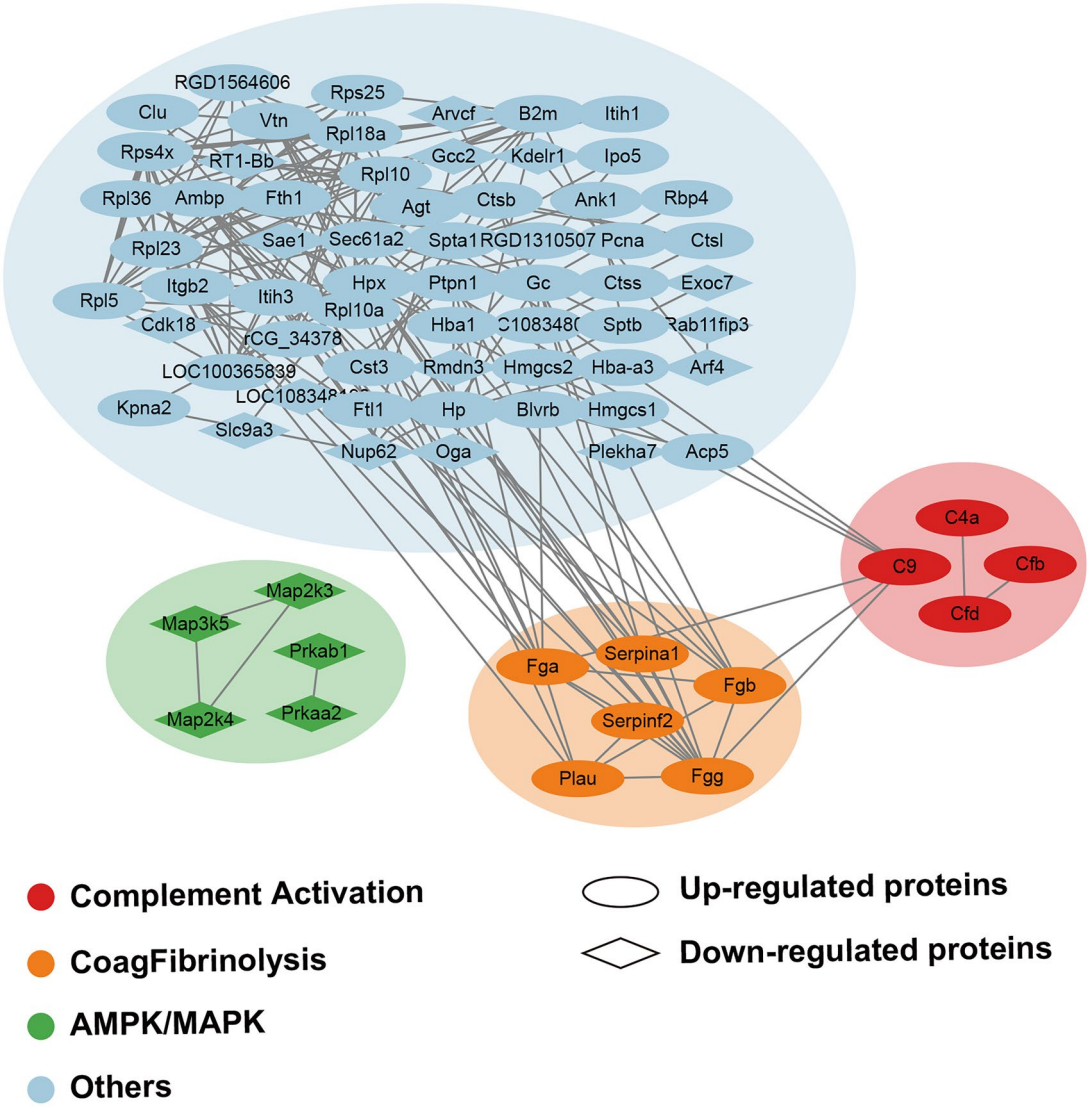

Figure 4. Protein–protein interaction network in the renal tissues of CI-AKI rats. All abbreviations are in Tables 1 and 2.

fibrinogen-related signal in CI-AKI kidneys, predominantly within tubular compartments and in regions of tubular injury (Figure 6(B)). To provide a more fibrin-specific histologic readout, MSB staining demonstrated increased fibrin-positive intraluminal deposits and casts in CI-AKI compared with Sham (Figure 6(C)). Masson's trichrome staining further revealed prominent intratubular casts and obstructive material in CI-AKI kidneys (Figure 6(D)), supporting the presence of proteinaceous luminal obstruction, albeit without fibrin specificity. RT-qPCR further showed increased renal expression of Serpina1 and Serpinf2 mRNAs in the CI-AKI group (Figure 6(E)), consistent with reduced fibrinolytic capacity and remodeling of the coagulation–fibrinolysis axis during CI-AKI. Collectively, these findings indicate a procoagulant and potentially pro-occlusive microenvironment in CI-AKI kidneys that may contribute to regional hypoperfusion.

3.4.3. Energy metabolism

RT-qPCR of renal tissues demonstrated downregulation of PRKAA2 (AMPKα2) and PRKAB1 (AMPKβ1), key regulators of cellular energy homeostasis, in CI-AKI (Figure 7(A)). The renal tissues of CI-AKI rats also had a decreased level of *Hnf4a* mRNA (a transcription factor for fatty acid oxidation), indicating dysregulation of lipid metabolism (Figure 7(B)). Using scanning electron microscopy, we found that in CI-AKI rats, kidney mitochondria exhibited excessive fission and fragmentation (Figure 7(C)). ELISA of renal tissues also demonstrated decreased levels of CAT, SOD, and GSH, and an increased level of MDA in CI-AKI rats (Figure 7(D)), indicative of increased oxidative stress. DHE fluorescence (indicative of ROS) was also

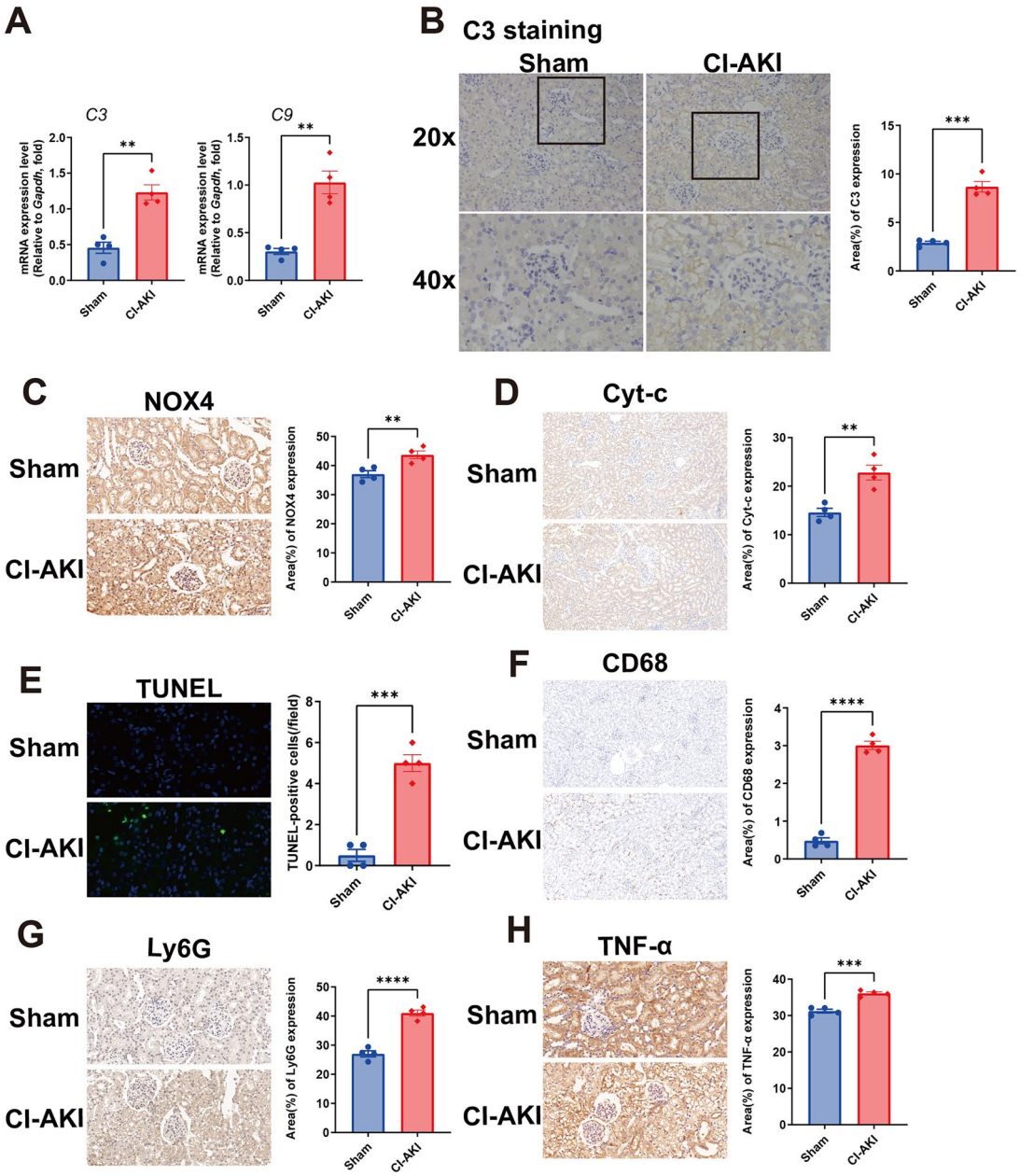

Figure 5. Effect of CI-AKI on complement activation, oxidative stress, and inflammation in rat renal tissues. RT-qPCR of *C3* and *C9* (A), immunohistochemistry of C3 (B), immunohistochemistry of NOX4 (C), immunohistochemistry of CYT-C (D), apoptosis (TUNEL assay) (E), immunohistochemistry of CD68 (F), immunohistochemistry of LY6G (G), and immunohistochemistry of TNF-A (H). Data are expressed as mean ± SEM. Independent-sample t test ($n = 4$ per group $^{*}p < 0.05$, $^{**}p < 0.01$, and $^{***}p < 0.001$).

markedly increased in CI-AKI kidneys, particularly in proximal tubules (Figure 7(E)). The decreased level of *Map2k4* mRNA (a kinase involved in stress signaling) suggested a compromised ability to respond to stress (Figure 7(F)).

4. Discussion

CI-AKI, also referred to as contrast-associated acute kidney injury (CA-AKI), remains a clinically important complication after iodinated contrast exposure in high-risk patients, and risk-stratification tools have been developed to support peri-procedural decision-making and prevention strategies [44]. However, the pathophysiological mechanisms of CI-AKI remain incompletely defined, CI-AKI-specific biomarkers are not

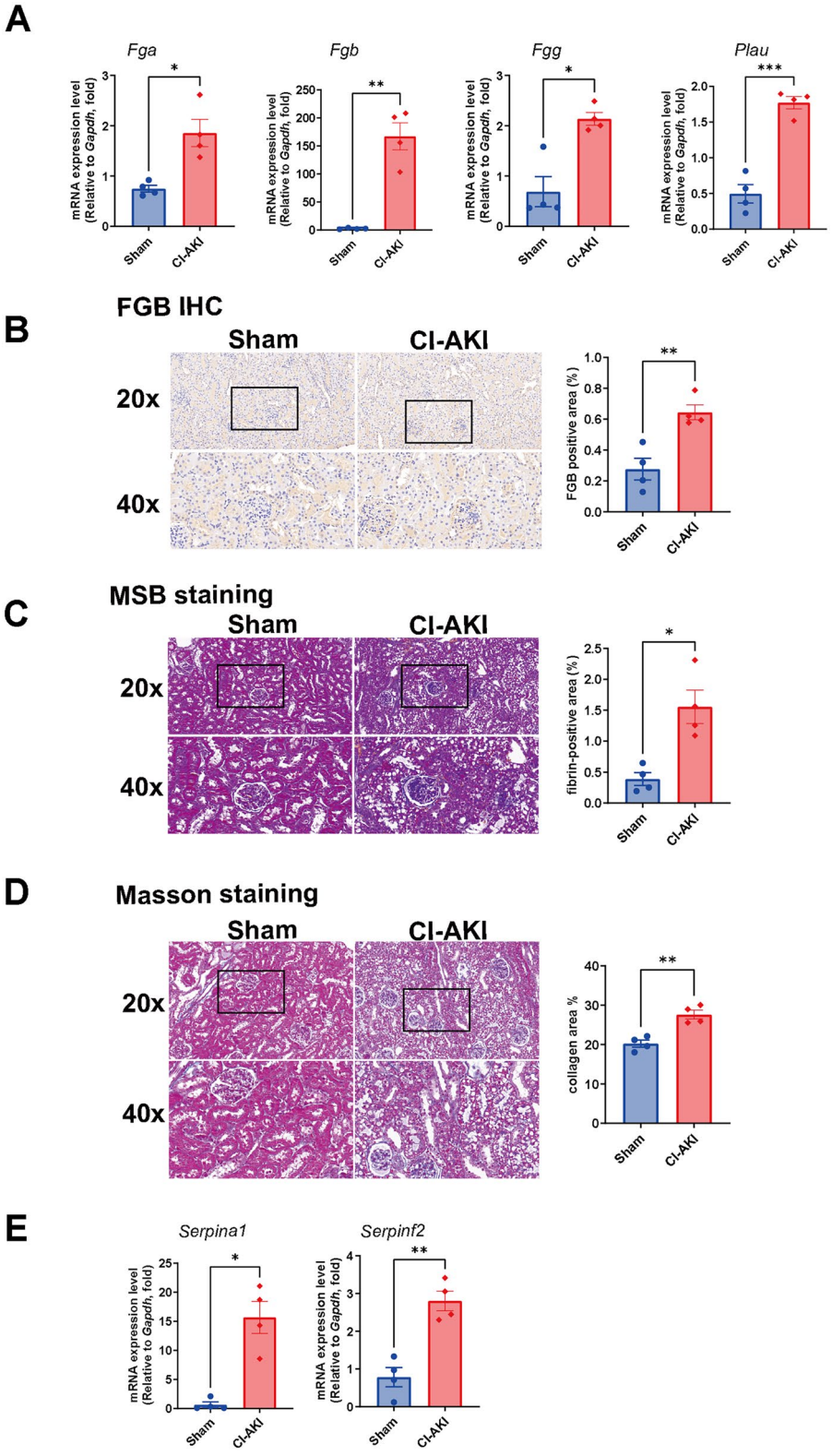

Figure 6. Effect of CI-AKI on microcirculatory obstruction in rat renal tissues. RT-qPCR for *Fga*, *Fgb*, *Fgg*, and *Plau* (A), Immunohistochemistry of FGB (B), MSB staining and quantification of fibrin-positive area (C), Masson staining and quantification of collagen (D), and RT-qPCR for *Serpina1* and *Serpinf2* (E). Data are expressed as mean ± SEM. Independent-sample t test ($n = 4$ per group $^{*}p < 0.05$, $^{**}p < 0.01$, and $^{***}p < 0.001$).

widely validated for routine use, and there is no universally accepted pharmacologic prevention or treatment strategy. In this study, we successfully established a rat model that recapitulates key features of human CI-AKI, including renal congestion and elevations in SCr, BUN, KIM-1, and NGAL [12]. Using 4D

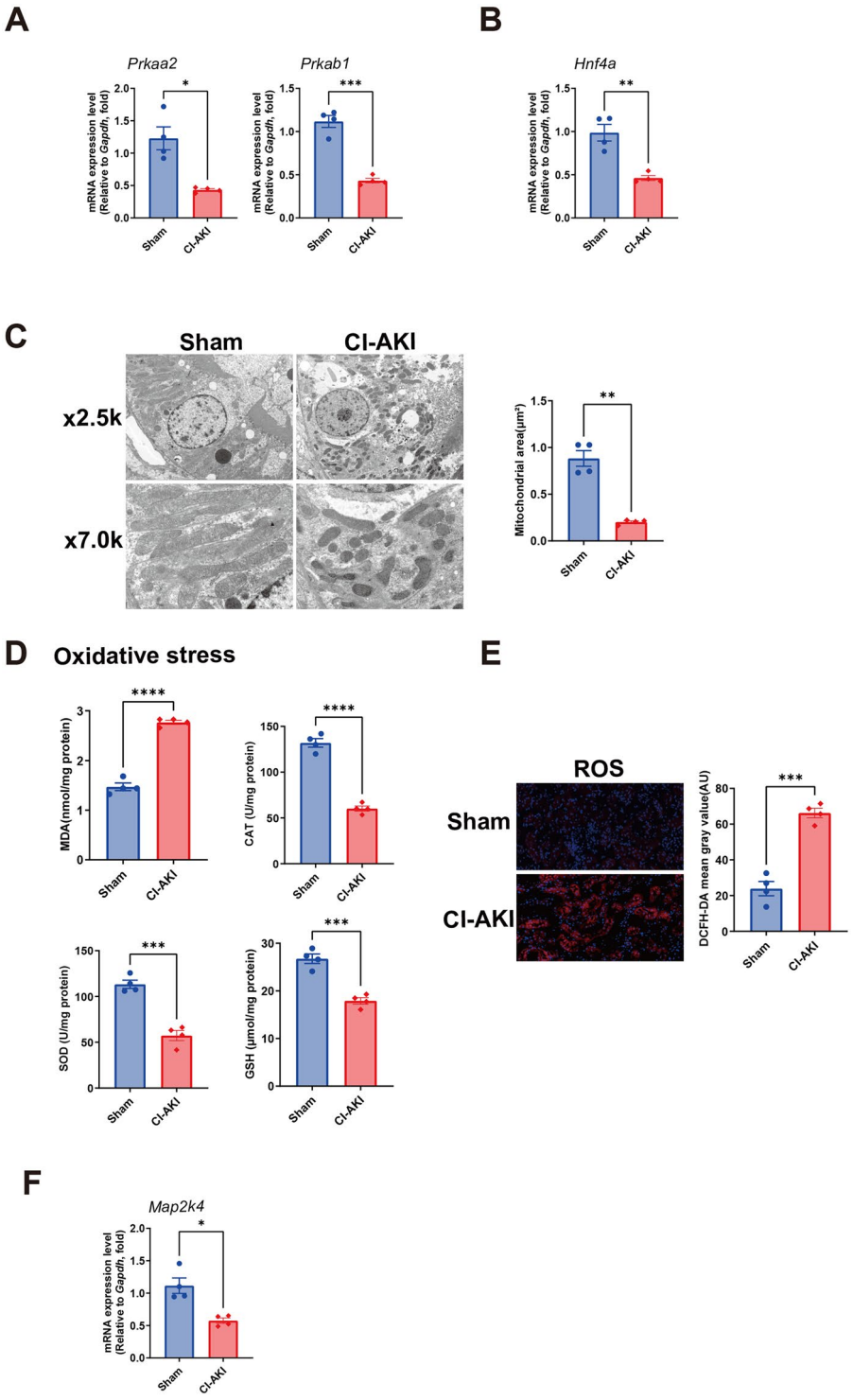

Figure 7. Effect of CI-AKI on energy metabolism and tubular injury in rat renal tissues. RT-qPCR for *Prkaa2*, *Prkab1*, and *Hnf4a* mRNAs (A, B), Representative electron micrographs of renal mitochondria (C), ELISA for CAT, SOD, and GSH, and MDA (D), ROS (E) and RT-qPCR for *Map2k4* (F). Data are expressed as mean ± SEM. Independent-sample t test ($n = 4$ per group *$p < 0.05$, **$p < 0.01$, and ***$p < 0.001$).

LC–MS/MS-based proteomics combined with bioinformatics analyses, we systematically characterized renal protein alterations associated with CI-AKI.

Our LC–MS/MS untargeted analysis of the renal proteome in CI-AKI and control rats provides insights into the complex pathophysiology of CI-AKI. In particular, we observed coordinated changes involving complement-related proteins (C3/C5 convertase-related proteins and terminal pathway components such

as C9; a C4 isoform annotated as C4a), coagulation/fibrinolysis factors (FGA, FGB, FGG, PLAU, SERPINA1, SERPINF2), and reduced abundance of key components in AMPK signaling (HNF4α, AMPK, PRKAA2, PRKAB1) and MAPK signaling (MAP2K3, MAP2K4, MAP3K5, A-RAF). These patterns are consistent with a multidimensional injury network in CI-AKI, linking inflammatory and hemostatic remodeling with impaired metabolic adaptation. Overall, a unifying interpretation is that these programs converge on microvascular dysfunction, where impaired peritubular capillary perfusion can generate spatially heterogeneous hypoxia and oxidant stress that amplify tubular injury [45]. This framework is consistent with the concept that reduced NO bioavailability together with oxidative stress forms a reinforcing loop that worsens endothelial function and regional oxygen delivery after contrast exposure [46].

Although complement activation has not been explicitly reported in humans with CI-AKI, our data suggest engagement of complement-related programs in a rat model of CI-AKI. It should be noted that in rodents, C4 isoforms do not map directly onto the human C4A/C4B nomenclature; therefore, the detected protein annotated as C4a should be interpreted as evidence of complement activation rather than assignment to a specific complement pathway. In agreement, another study of C3 knockout mice with ischemia-reperfusion injury reported these mice experienced alleviation of renal injury, decreased infiltration of neutrophils, and decreased formation of neutrophil extracellular traps (NETs) [47]. An *in vitro* study reported that C5A led to increased production of NETs when added to human neutrophils [48]. A recent study found that C5A was associated with increased production of ROS in mitochondria [49], and related *in vitro* experiments, in which human neutrophils were exposed to C5A, showed that this treatment led to increased shedding of microvesicles and a decreased level of the neutrophil C5A receptor (C5aR1) [49]. Collectively, these observations support a testable hypothesis wherein complement activation may amplify CI-AKI through innate immune effector mechanisms, with NETs formation serving as a plausible mechanistic bridge linking complement-driven inflammation to microvascular obstruction – a premise warranting direct validation in CI-AKI [50].

Activation of the coagulation cascade can further contribute to a self-amplifying cycle of renal dysfunction in CI-AKI, in which platelet activation and thrombin generation promote thrombosis and inflammatory signaling [51,52] through increased thrombin generation [53]. Activated platelets release cytokines and chemokines that facilitate recruitment of leukocytes and other immune cells, followed by endothelial activation and microvascular injury. This microvascular injury can further aggravate thrombosis, while the resulting inflammatory milieu exacerbates tubular epithelial stress and injury. Within this framework, immunothrombosis-driven capillary plugging can be interpreted as a microvascular amplifier that reinforces endothelial dysfunction and regional hypoxia, thereby sustaining oxidant stress in injured tubules [46].

Importantly, although Masson's trichrome staining indicates proteinaceous and extracellular matrix–rich casts, it does not specifically identify fibrin. To address this limitation, we performed MSB staining and IHC for fibrinogen β chain (FGB), which confirmed fibrin(ogen)-rich intratubular and/or intrarenal deposits. These findings support the presence of immunothrombotic microvascular occlusion rather than nonspecific cast formation. Together with venous congestion, these observations raise the possibility of a renal 'no-reflow-like' state.

We analyzed the PPI target networks of DEPs using STRING, and identified three hub DEPs, two with up-regulation (complement activation and coagulation/fibrinolysis) and one with downregulation AMPK/MAPK signaling (Figure 4). Among the upregulated proteins, the fibrinogen gamma chain, fibrinogen alpha chain, and fibrinogen beta chain represented central nodes in the network. Previous research showed that serum the fibrinogen level is positively associated with cardiovascular disease [54,55]. Fibrinogen also has an important function in diverse physiological processes that are vital to renal processes. For example, fibrinogen is a biomarker for AKI in patients who received repair of an abdominal aortic aneurysm due to its high immunoreactivity in the kidney and urine [56]. Fibrinogen is also classified as an acute response protein because it has an important role in tissue injury, in that thrombin-mediated cleavage of fibrinogen with other acute inflammatory responses can modulate inflammatory responses [57]. An increased fibrinogen level is also associated with increased blood viscosity, and the resulting increase of shear stress can decrease the function of endothelial cells [58]. The fibrinogen-induced increase in blood viscosity can lead to tubular hypoperfusion and hypoxia, and then AKI [10]. Thus, fibrinogen accumulation may not only serve as a risk stratification biomarker for CI-AKI but also directly contribute to renal injury through adverse effects on microvascular perfusion.

In contrast, downregulation of AMPK and MAPK signaling pathways suggests impaired cellular energy sensing and stress adaptation in CI-AKI [59,60]. AMPK is a central regulator of cellular metabolism and mitochondrial homeostasis, and its suppression may compromise adaptive responses to hypoxia and oxidative stress [61,62]. MAPK signaling exhibits context- and cell-type–dependent effects; while certain MAPKs promote inflammation when activated, basal MAPK activity in tubular epithelial cells may be required for stress tolerance and survival following ischemic or toxic injury [43,63]. Suppression of these pathways may therefore predispose tubular epithelial cells to maladaptive responses, potentially including ferroptosis driven by lipid peroxidation and disrupted redox homeostasis [64].

From a translational perspective, mapping deregulated protein programs to existing drug classes may help prioritize rational repurposing hypotheses. Complement-directed approaches are conceptually appealing because excessive complement activation can amplify inflammation, endothelial dysfunction, and tubular injury, and complement is increasingly recognized as both a candidate biomarker axis and a potential therapeutic target in AKI more broadly [33]. Notably, clinical trials of recombinant human C1 esterase inhibitor in contrast-induced AKI have demonstrated limited efficacy, underscoring the importance of defining the relevant complement triggers, optimal treatment timing, and the most appropriate level of pathway intervention [33]. In parallel, our coagulation–fibrinolysis signature supports consideration of strategies aimed at restoring fibrinolytic capacity, with careful attention to bleeding risk; for example, augmentation of endogenous fibrinolysis with intravenous Glu-plasminogen has been reported to attenuate thrombotic angiopathy-associated AKI in experimental settings without observed bleeding complications in that model [65].

In clinical practice, CA-AKI/CI-AKI risk prediction is still largely based on clinical characteristics and peri-procedural variables, as reflected by a contemporary, parsimonious PCI risk score [44]. Our findings support the hypothesis that incorporating mechanistically anchored markers – such as fibrinogen chains and SERPINA1, provided they are detectable in plasma or urine and exhibit appropriate temporal dynamics relative to injury – could complement existing models and enhance biologically informed risk stratification, a premise that requires prospective clinical validation.

Future work should prioritize translational validation of the complement–coagulation/fibrinolysis–metabolic signaling signature in human CI-AKI cohorts across diverse clinical contexts, with enrichment for high-risk populations (diabetes, CKD, heart failure) and standardized timing relative to contrast exposure. Integrated multi-omics with spatial and temporal resolution (proteomics, metabolomics, single-cell/spatial transcriptomics) will be important to localize pathway activation to specific compartments and cell types, and to clarify crosstalk among tubular epithelium, endothelium, and infiltrating myeloid cells. Mechanistic studies employing genetic or pharmacologic perturbation of key nodes – including components of the C3/C5 convertase, fibrinogen and SERPINA1, and the AMPK and MAPK pathways – are warranted to test causality, define therapeutic windows, and determine whether NETs formation and microvascular 'no-reflow-like' hypoperfusion act as actionable downstream amplifiers of injury. Finally, longitudinal and biomarker-guided studies should assess whether early pathway modulation mitigates AKI severity and limits transition to CKD, and whether fibrinogen/SERPINA1 and related markers can enable mechanism-informed risk stratification and precision prevention; in parallel, dedicated profiling of lipid peroxidation and ferroptosis regulators (e.g. GPX4/SLC7A11/ACSL4, 4-HNE adducts) may refine downstream cell-death hypotheses.

5. Conclusion

In summary, comprehensive proteomic profiling of a rat model of CI-AKI suggests that disease pathogenesis involves a complex, multidimensional injury network (Figure 8). Excessive activation of the complement cascade is associated with inflammatory injury and oxidative stress, while dysregulation of coagulation and fibrinolysis – characterized by fibrinogen accumulation and impaired fibrinolysis – may contribute to immunothrombotic microvascular occlusion, regional ischemic hypoxia, and tubular epithelial cell injury. Concurrent suppression of AMPK and MAPK signaling is consistent with impaired cellular energy metabolism and stress adaptation, potentially exacerbating renal injury. Together, these findings

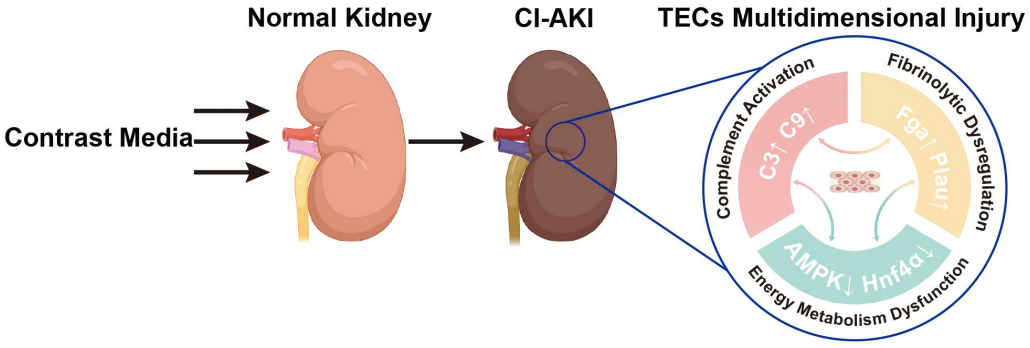

Figure 8. Administration of iohexol contrast medium to rats leads to CI-AKI due to multidimensional injury of tubular epithelial cells.

support the concept that microvascular immunothrombosis may act as an important injury amplifier in CI-AKI and raise the possibility that targeted modulation of complement activation, restoration of fibrinolytic balance, and reactivation of metabolic repair pathways could represent therapeutic hypotheses worthy of further testing. Moreover, fibrinogen and SERPINA1 may serve as mechanistically informed biomarkers for improved risk stratification and precision prevention of CI-AKI.

Author contributions

CRediT: **Qiang Yang**: Data curation, Formal analysis, Investigation, Methodology, Validation, Visualization, Writing – original draft; **Liming Sun**: Data curation, Formal analysis, Investigation, Methodology, Resources, Visualization, Writing – original draft; **Zhijian Zhang**: Conceptualization, Funding acquisition, Project administration, Resources, Supervision, Writing – review & editing; **Zhixin Yan**: Investigation, Validation; **Jian Zhang**: Investigation, Resources; **Jiachang Hu**: Conceptualization, Data curation, Formal analysis, Methodology, Project administration, Resources, Supervision, Writing – review & editing; **Xiaoqiang Ding**: Conceptualization, Funding acquisition, Project administration, Resources, Supervision, Writing – review & editing.

Disclosure statement

No potential conflict of interest was reported by the authors.

Funding

The study was funded by National Key Research and Development Program-Intergovernmental International Scientific and Technological Innovation Cooperation (2024YFE0199600), the National Natural Science Foundation of China grants (82470717) (82370685) and Top Talent Support Program for young and middle-aged people of Wuxi Health Committee (NO: BJ2023009).

ORCID

Qiang Yang http://orcid.org/0000-0002-3414-469X
Liming Sun http://orcid.org/0009-0001-5089-0975
Zhijian Zhang http://orcid.org/0009-0001-5441-532X
Zhixin Yan http://orcid.org/0009-0002-2768-8645
Jian Zhang http://orcid.org/0000-0003-0354-1593
Jiachang Hu http://orcid.org/0000-0003-0262-0935
Xiaoqiang Ding http://orcid.org/0000-0002-3312-4056

Data availability statement

The data that support the findings of this study are openly available in iProX at (https://www.iprox.cn/page/DSV021.html;?url=1764119451830Udj5, keyword: yn4w), reference number IPX0014404001.

References

[1] Mettler FA, Jr., Mahesh M, Bhargavan-Chatfield M, et al. Patient exposure from radiologic and nuclear medicine procedures in the united states: procedure volume and effective dose for the period 2006–2016. Radiology. 2020;295(2):418–427. doi: 10.1148/radiol.2020192256.

[2] Seeliger E, Sendeski M, Rihal CS, et al. Contrast-induced kidney injury: mechanisms, risk factors, and prevention. Eur Heart J. 2012;33(16):2007–2015. doi: 10.1093/eurheartj/ehr494.

[3] Chaikijurajai T, Demirjian S, Tang WHW. Prognostic value of natriuretic peptide levels for adverse renal outcomes in patients with moderate to severe acute kidney injury with or without heart failure. J Am Heart Assoc. 2023;12(21):e031453. doi: 10.1161/JAHA.123.031453.

[4] Mehta RL, Cerdá J, Burdmann EA, et al. International Society of Nephrology's 0by25 initiative for acute kidney injury (zero preventable deaths by 2025): a human rights case for nephrology. Lancet. 2015;385(9987):2616–2643. doi: 10.1016/S0140-6736(15)60126-X

[5] Mehran R, Dangas GD, Weisbord SD. Contrast-associated acute kidney injury. N Engl J Med. 2019;380(22):2146–2155. doi: 10.1056/NEJMra1805256.

[6] Mccullough PA, Choi JP, Feghali GA, et al. Contrast-induced acute kidney injury. J Am Coll Cardiol. 2016;68(13):1465–1473. doi: 10.1016/j.jacc.2016.05.099.

[7] Zhou LY, Liu K, Yin WJ, et al. Arginase2 mediates contrast-induced acute kidney injury via facilitating nitrosative stress in tubular cells. Redox Biol. 2023;67:102929. doi: 10.1016/j.redox.2023.102929.

[8] Wang Z, Wang Q, Gong X. Unveiling the mysteries of contrast-induced acute kidney injury: new horizons in pathogenesis and prevention. Toxics. 2024;12(8):620. doi: 10.3390/toxics12080620.

[9] Katzberg RW. Contrast medium-induced nephrotoxicity: which pathway? Radiology. 2005;235(3):752–755. doi: 10.1148/radiol.2353041865.

[10] Persson PB, Hansell P, Liss P. Pathophysiology of contrast medium-induced nephropathy. Kidney Int. 2005;68(1):14–22. doi: 10.1111/j.1523-1755.2005.00377.x.

[11] Deng J, Wu G, Yang C, et al. Rosuvastatin attenuates contrast-induced nephropathy through modulation of nitric oxide, inflammatory responses, oxidative stress and apoptosis in diabetic male rats. J Transl Med. 2015;13(1):53. doi: 10.1186/s12967-015-0416-1.

[12] Yang Q, Hu J, Ning Y, et al. A NOVEL RAT MODEL OF CONTRAST-INDUCED ACUTE KIDNEY INJURY BASED ON RENAL CONGESTION AND THE RENO-PROTECTION OF MITOCHONDRIAL FISSION INHIBITION. Shock. 2023;59(6):930–940. doi: 10.1097/SHK.0000000000002125.

[13] Zhang L, Cao X, Yang Y, et al. Risk prediction models for contrast-induced acute kidney injury in patients with acute coronary syndromes: a systematic review and meta-analysis. Front Med (Lausanne). 2025;12:1629369. doi: 10.3389/fmed.2025.1629369.

[14] Peng L, Li S, Huang Q, et al. Irisin-mediated muscle-renal crosstalk as a protective mechanism against contrast-induced acute kidney injury via cGAS-STING signalling inhibition. Clin Transl Med. 2025;15(3):e70235. doi: 10.1002/ctm2.70235.

[15] Wang H, Gao T, Zhang R, et al. The intellectual base and global trends in contrast-induced acute kidney injury: a bibliometric analysis. Ren Fail. 2023;45(1):2188967. doi: 10.1080/0886022X.2023.2188967.

[16] James MT, Har BJ, Tyrrell BD, et al. Effect of clinical decision support with audit and feedback on prevention of acute kidney injury in patients undergoing coronary angiography: a randomized clinical trial. JAMA. 2022;328(9):839–849. doi: 10.1001/jama.2022.13382.

[17] Liu C, Liu C, Liu GJ, et al. BE-43547A(2) exerts hypoxia-selective inhibition on human pancreatic cancer cells through targeting eEF1A1 and disrupting its association with FoxO1. Acta Pharmacol Sin. 2025;46(5):1433–1444. doi: 10.1038/s41401-024-01461-y.

[18] Li HS, Zhou YN, Li L, et al. HIF-1α protects against oxidative stress by directly targeting mitochondria. Redox Biol. 2019;25:101109. doi: 10.1016/j.redox.2019.101109.

[19] Langley SR, Dwyer J, Drozdov I, et al. Proteomics: from single molecules to biological pathways. Cardiovasc Res. 2013;97(4):612–622. doi: 10.1093/cvr/cvs346.

[20] Wang Y, Li J, Lu D, et al. Integrated proteome and phosphoproteome analysis of interscapular brown adipose and subcutaneous white adipose tissues upon high fat diet feeding in mouse. J Proteomics. 2022;255:104500. doi: 10.1016/j.jprot.2022.104500.

[21] Sherman BT, Panzade G, Imamichi T, et al. DAVID Ortholog: an integrative tool to enhance functional analysis through orthologs. Bioinformatics. 2024;40(10):btae615. doi: 10.1093/bioinformatics/btae615.

[22] Campbell RE, Chen CH, Edelstein CL. Overview of antibiotic-induced nephrotoxicity. Kidney Int Rep. 2023;8(11):2211–2225. doi: 10.1016/j.ekir.2023.08.031.

[23] Asrani SK, Shankar N, Da Graca B, et al. Role of novel kidney biomarkers in patients with cirrhosis and after liver transplantation. Liver Transpl. 2022;28(3):466–482. doi: 10.1002/lt.26344.

[24] Ba Aqeel SH, Sanchez A, Batlle D. Angiotensinogen as a biomarker of acute kidney injury. Clin Kidney J. 2017;10(6):759–768. doi: 10.1093/ckj/sfx087.

[25] Zou C, Wang C, Lu L. Advances in the study of subclinical AKI biomarkers. Front Physiol. 2022;13:960059. doi: 10.3389/fphys.2022.960059.

[26] Tan J, Yin K, Ouyang Z, et al. Real-time monitoring renal impairment due to drug-induced AKI and diabetes-caused CKD using an NAG-activatable NIR-II nanoprobe. Anal Chem. 2021;93(48):16158–16165. doi: 10.1021/acs.analchem.1c03926.
[27] Du S, Tian J, Xiao Z, et al. Serum alpha 1-antitrypsin predicts severe acute kidney injury after cardiac surgery. J Thorac Dis. 2019;11(12):5053–5062. doi: 10.21037/jtd.2019.12.17.
[28] Dihazi H, Koziolek MJ, Datta RR, et al. FABP1 and FABP3 have high predictive values for renal replacement therapy in patients with acute kidney injury. Blood Purif. 2016;42(3):202–213. doi: 10.1159/000447115.
[29] Graw JA, Hildebrandt P, Krannich A, et al. The role of cell-free hemoglobin and haptoglobin in acute kidney injury in critically ill adults with ARDS and therapy with VV ECMO. Crit Care. 2022;26(1):50. doi: 10.1186/s13054-022-03894-5.
[30] Li S, Zhang Y, Lu R, et al. Peroxiredoxin 1 aggravates acute kidney injury by promoting inflammation through Mincle/Syk/NF-κB signaling. Kidney Int. 2023;104(2):305–323. doi: 10.1016/j.kint.2023.04.013.
[31] Bongoni AK, Kiss B, Mcrae JL, et al. Targeting the complement lectin pathway with a highly specific MASP-2 inhibitor protects against renal ischemia-reperfusion injury. Proc Natl Acad Sci U S A. 2025;122(16):e2424754122. doi: 10.1073/pnas.2424754122.
[32] Xue YR, Yao S, Liu Q, et al. Dihydro-stilbene gigantol relieves CCl(4)-induced hepatic oxidative stress and inflammation in mice via inhibiting C5b-9 formation in the liver. Acta Pharmacol Sin. 2020;41(11):1433–1445. doi: 10.1038/s41401-020-0406-6.
[33] Wei L, Garces JPD, Kashani M, et al. Role of the complement system in acute kidney injury: a narrative review. Mayo Clin Proc. 2025;100(10):1796–1809. doi: 10.1016/j.mayocp.2025.06.005.
[34] Zhang P, Sun C, Mo S, et al. Salvaging donated kidneys from prolonged warm ischemia during ex vivo hypothermic oxygenated perfusion. Kidney Int. 2024;106(2):273–290. doi: 10.1016/j.kint.2024.04.018.
[35] Song C, Qiao Z, Chen L, et al. Identification of key genes as early warning signals of acute myocardial infarction based on weighted gene correlation network analysis and dynamic network biomarker algorithm. Front Immunol. 2022;13:879657. doi: 10.3389/fimmu.2022.879657.
[36] Lahmar Z, Ahmed E, Fort A, et al. Hedgehog pathway and its inhibitors in chronic obstructive pulmonary disease (COPD). Pharmacol Ther. 2022;240:108295. doi: 10.1016/j.pharmthera.2022.108295.
[37] Al Dawood R, Hayward CPM. Laboratory diagnosis of congenital and acquired coagulopathies, including challenging-to-diagnose rare bleeding disorders. Pathology. 2025;57(6):687–695. doi: 10.1016/j.pathol.2025.06.004.
[38] Tong CC, Xue YF, He X, et al. Mitochondrial dysfunction-mediated hepatocyte senescence is involved in cholestatic liver injury. Free Radic Biol Med. 2025;239:528–539. doi: 10.1016/j.freeradbiomed.2025.08.006.
[39] Malik N, Shaw RJ. The AMPK pathway: molecular rejuvenation of metabolism and mitochondria. Annu Rev Cell Dev Biol. 2025;41(1):375–402. doi: 10.1146/annurev-cellbio-120420-094431.
[40] Liu Y, Zou M, Wang Y. The lipid-oxidative stress axis: novel therapeutic targets for podocytopathy. J Inflamm Res. 2025;18:12505–12532. doi: 10.2147/JIR.S530737.
[41] Xiao X, Li R, Cui B, et al. Liver ACSM3 deficiency mediates metabolic syndrome via a lauric acid-HNF4α-p38 MAPK axis. EMBO J. 2024;43(4):507–532. doi: 10.1038/s44318-023-00020-1.
[42] Lees J, Pèrtille F, Løtvedt P, et al. The mitoepigenome responds to stress, suggesting novel mito-nuclear interactions in vertebrates. BMC Genomics. 2023;24(1):561. doi: 10.1186/s12864-023-09668-9.
[43] Kyriakis JM, Avruch J. Mammalian MAPK signal transduction pathways activated by stress and inflammation: a 10-year update. Physiol Rev. 2012;92(2):689–737. doi: 10.1152/physrev.00028.2011.
[44] Mehran R, Owen R, Chiarito M, et al. A contemporary simple risk score for prediction of contrast-associated acute kidney injury after percutaneous coronary intervention: derivation and validation from an observational registry. Lancet. 2021;398(10315):1974–1983. doi: 10.1016/S0140-6736(21)02326-6
[45] Wu L, Gokden N, Mayeux PR. Evidence for the role of reactive nitrogen species in polymicrobial sepsis-induced renal peritubular capillary dysfunction and tubular injury [J]. J Am Soc Nephrol. 2007;18(6):1807–1815. doi: 10.1681/ASN.2006121402.
[46] Zoccali C, Mallamaci F. Inorganic nitrate: a game changer in preventing contrast-associated acute kidney injury. Eur Heart J. 2024;45(18):1659–1661. doi: 10.1093/eurheartj/ehae094.
[47] Wu X, You D, Cui J, et al. Reduced neutrophil extracellular trap formation during ischemia reperfusion injury in C3 KO mice: c 3 requirement for NETs release. Front Immunol. 2022;13:781273. doi: 10.3389/fimmu.2022.781273.
[48] Chen Y, Li X, Lin X, et al. Complement C5a induces the generation of neutrophil extracellular traps by inhibiting mitochondrial STAT3 to promote the development of arterial thrombosis. Thromb J. 2022;20(1):24. doi: 10.1186/s12959-022-00384-0.
[49] Karasu E, Demmelmaier J, Kellermann S, et al. Complement C5a induces pro-inflammatory microvesicle shedding in severely injured patients. Front Immunol. 2020;11:1789. doi: 10.3389/fimmu.2020.01789.
[50] Fu Y, Wang W, Gong N, et al. Neutrophil and neutrophil extracellular traps in acute kidney injury: from mechanisms to treatments. Front Immunol. 2025;16:1688207. doi: 10.3389/fimmu.2025.1688207.
[51] Allam R, Scherbaum CR, Darisipudi MN, et al. Histones from dying renal cells aggravate kidney injury via TLR2 and TLR4. J Am Soc Nephrol. 2012;23(8):1375–1388. doi: 10.1681/ASN.2011111077.
[52] Allam R, Darisipudi MN, Tschopp J, et al. Histones trigger sterile inflammation by activating the NLRP3 inflammasome. Eur J Immunol. 2013;43(12):3336–3342. doi: 10.1002/eji.201243224.

[53] Ammollo CT, Semeraro F, Xu J, et al. Extracellular histones increase plasma thrombin generation by impairing thrombomodulin-dependent protein C activation. J Thromb Haemost. 2011;9(9):1795–1803. doi: 10.1111/j.1538-7836.2011.04422.x.
[54] Stec JJ, Silbershatz H, Tofler GH, et al. Association of fibrinogen with cardiovascular risk factors and cardiovascular disease in the Framingham Offspring Population. Circulation. 2000;102(14):1634–1638. doi: 10.1161/01.cir.102.14.1634.
[55] Carty CL, Cushman M, Jones D, et al. Associations between common fibrinogen gene polymorphisms and cardiovascular disease in older adults. The Cardiovascular Health Study. Thromb Haemost. 2008;99(2):388–395. doi: 10.1160/TH07-08-0523.
[56] Goldshmit Y, Matteo R, Sztal T, et al. Blockage of lysophosphatidic acid signaling improves spinal cord injury outcomes. Am J Pathol. 2012;181(3):978–992. doi: 10.1016/j.ajpath.2012.06.007.
[57] Luyendyk JP, Schoenecker JG, Flick MJ. The multifaceted role of fibrinogen in tissue injury and inflammation. Blood. 2019;133(6):511–520. doi: 10.1182/blood-2018-07-818211.
[58] Ozcan Cetin EH, Könte HC, Temizhan A. Blood viscosity should not be overlooked when evaluating the fibrinogen to albumin ratio. Angiology. 2019;70(5):465–466. doi: 10.1177/0003319718822244.
[59] Herzig S, Shaw RJ. AMPK: guardian of metabolism and mitochondrial homeostasis. Nat Rev Mol Cell Biol. 2018;19(2):121–135. doi: 10.1038/nrm.2017.95.
[60] Hall AM, Schuh CD. Mitochondria as therapeutic targets in acute kidney injury. Curr Opin Nephrol Hypertens. 2016;25(4):355–362. doi: 10.1097/MNH.0000000000000228.
[61] Declèves AE, Sharma K. Novel targets of antifibrotic and anti-inflammatory treatment in CKD. Nat Rev Nephrol. 2014;10(5):257–267. doi: 10.1038/nrneph.2014.31.
[62] Dugan LL, You YH, Ali SS, et al. AMPK dysregulation promotes diabetes-related reduction of superoxide and mitochondrial function. J Clin Invest. 2013;123(11):4888–4899. doi: 10.1172/JCI66218.
[63] Johnson GL, Lapadat R. Mitogen-activated protein kinase pathways mediated by ERK, JNK, and p38 protein kinases. Science (1979). 2002;298(5600):1911–1912. doi: 10.1126/science.1072682.
[64] Matsui S, Yamamoto T, Takabatake Y, et al. Defective autophagy and AMPK inactivation drive ferroptosis in diabetic kidney disease. Diabetologia. 2026;69(3):815–832. doi: 10.1007/s00125-025-06612-2.
[65] Lyubenov L, Shi C, Zhao D, et al. Intravenous Glu-plasminogen attenuates cholesterol crystal embolism-induced thrombotic angiopathy, acute kidney injury and kidney infarction. Nephrol Dial Transplant. 2023;38(1):93–105. doi: 10.1093/ndt/gfac273.